Crystal defect evaluation of silicon carbide (SiC) using an electron microscope

Toshiyuki Isshiki

Kyoto Institute of Technology,
Department of Electrical Engineering and Electronics,
Professor

1. Introduction

Electric power is in wide use for information transmission equipment, such as computers and mobile telephones, as well as for use as an energy, heat, and light source, and it is now indispensable for human life. There is a strong requirement for more efficient use of electric power as part of a move toward a low-carbon society, and there are hopes for power management, involving application of power devices. Power devices are key components, used for electric power conversion and control, and silicon was used in the previously available devices. In recent years, attention has been given to power devices that use silicon carbide (SiC)[1] that reach beyond the limits of silicon power devices. SiC is a compound semiconductor in which silicon and carbon are bound in a 1:1 relationship, and it is characterized by strong interatomic bonds, and a wide band gap. SiC devices have even higher dielectric breakdown resistance than silicon, and can be used to achieve efficient power devices. However, one area of concern for the practical application of SiC devices relates to difficulties with the quality of SiC wafer crystals. During SiC crystal growth, localized loss of structural regularity occurs, and crystal defects, such as stacking faults and dislocation, occur readily. It is known that some such defects negatively affect the operation of devices. Therefore, in order to increase the yield and reliability of SiC devices, it is important to understand the locations and types of crystal defects. Our research group is currently investigating analysis methods for SiC crystal defects involving application of electron microscopy. The present report introduces methods for locating crystal defects that can be seen on wafer surfaces, using high-resolution scanning electron microscopy (SEM)[2]; and also methods for processing parts of wafers with crystal defects, using a focused ion beam processing and observation device (FIB), and determining the details of types of crystal defect using scanning transmission electron microscopy (STEM)[3, 4].

2. High-resolution evaluation of SiC wafer surfaces using SEM

As shown in Fig. 1, SiC devices are prepared by epitaxial growth of the basal plane, at an inclination solely in the angle termed the "off angle". Basal planes laid down sequentially on the epitaxial crystal surface are termed "terraces", and steps are formed at the ends of the terraces. Crystal growth progresses by adherence of atoms to the ends of these steps, so that the steps advance. As crystal growth progresses, the orientation of the wafer surface should ideally be consistent, and steps should be formed at approximately equal intervals[5]. This mechanism is termed "step-flow growth". We suspected that, if there are crystal defects on the crystal surface, there may be disorders of step flow in the vicinity, leading to changes in step morphology, and we therefore investigated the microscopic morphology of epitaxial crystal surfaces. The samples used in this research were commercially available SiC epitaxial wafers with off angles of 4º, minimum step heights of 1 nm, and terrace widths of 14 nm. In order to evaluate the morphologies of steps of this type, there is a need for observation techniques that have high (nanometer-order) resolution in both the horizontal and vertical directions. SEM is in wide use for evaluating the structures of sample

surfaces, but, in order to evaluate steps of nanometer-order height, it is essential for the electron beams with which the sample is irradiated to be at a low energy level (several hundred electron-volts)[6]. In recent years, it has become possible to carry out evaluations with field-emission SEM, under conditions of low irradiation energy, without loss of resolution.
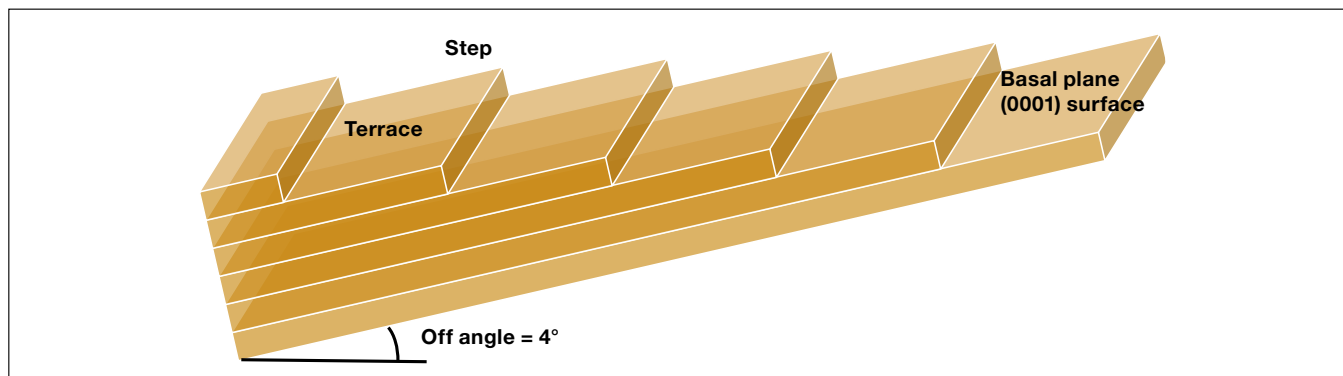

Fig. 1   Schematic diagram of the surface structure of SiC epitaxial crystals

In this research, evaluation was tried using an SU8220 (Hitachi High-Technologies Corporation; Fig. 2), with the irradiation energy being 500 eV. In addition, in order to detect electrons discharged from areas as close as possible to the sample surface, evaluation was carried out using a detector that detects low-emission-angle backscattered electrons.

Fig. 2   External view of SU8220

 [11]

The results of SEM evaluation of numerous visual fields of the wafer surface confirmed that the growth steps were aligned on the SiC epitaxial wafer surface at approximately equal intervals. In addition, it was shown that there are surface defects with unique step morphology, and that these are of two types, with one having triangular terraces, and the other having wide, parallel terraces. SEM images of the surface defects are shown in Fig. 3, with the step flow progressing from left to right. It can be seen in these SEM images that numerous fine, linear structures extend from above to below, and these are arranged at approximately regular intervals. They represent the growth steps, with the minimum inter-step interval being 10 to 20 nm. It is therefore considered that steps corresponding to a simple lattice can be observed by SEM. In Fig. 3 (a) and (b), the steps are inflected close to the centers of the images, and form triangular terraces. The length of each terrace is approximately 2 μm, in alignment with the step, and the terrace widths are 270 and 80 nm, respectively, in Fig.3 (a) and (b). Figure 3 (c) is an SEM image of the surface defects of parallel terrace morphology. A terrace 100 nm wide is formed here, crossing a region that is approximately 15 μm wise and aligned with the terrace. The upper end of the terrace converges, with approximate left-right symmetry, whereas at the lower end the steps at the downstream side of the step flow form a straight line, but the steps at the upstream side bend and converge.
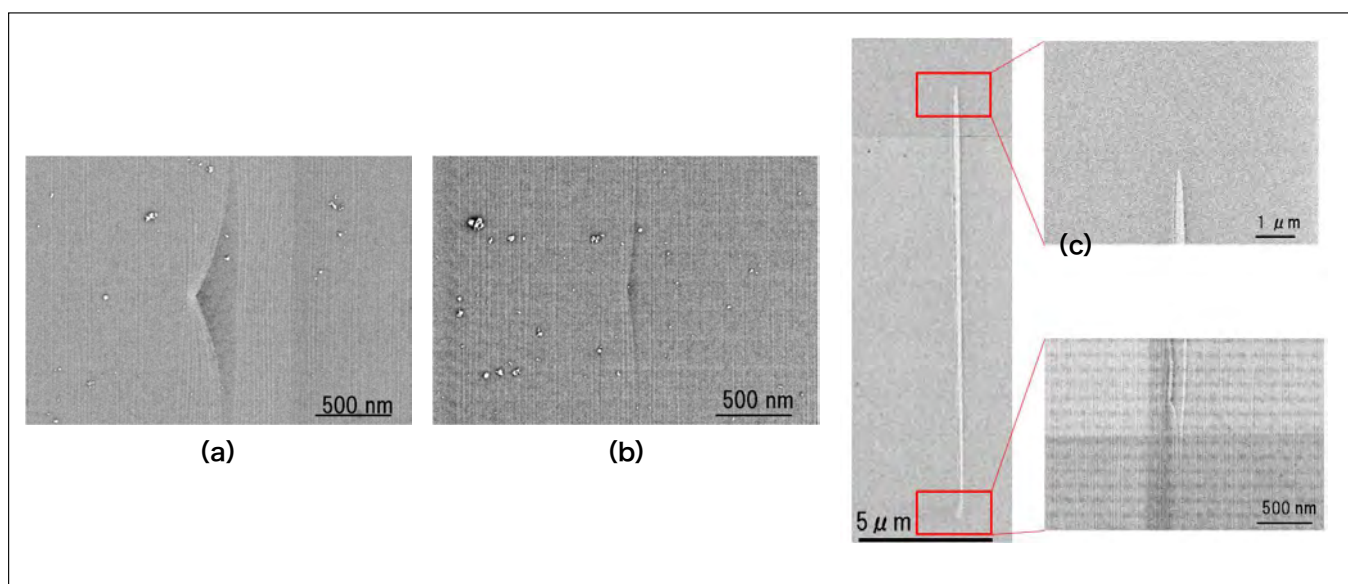

Fig. 3　SiC epitaxial wafer surface defects
(a) Surface defects with triangular terraces; terrace width: 270 nm
(b) Surface defects with triangular terraces; terrace width: 90 nm
(c) Surface defects with parallel terraces

Next, in order to confirm whether there is a relationship between surface defects and dislocations, the SiC wafer was subjected to etching treatment using high-temperature, molten potassium hydroxide. Molten potassium hydroxide etches in priority at loci where dislocations can be seen on the SiC wafer surface, and it forms pits, with the pit morphology varying according to the type of dislocation[7]. Figure 4 shows SEM images of the surface after etching, these being the results of evaluation of the same loci as those shown in Fig.3. In Fig. 4 (a) and (b), hexagonal etching pits were formed where the steps were inflected in Fig. 3 (a) and (b). On the basis of pit morphology, it is considered that triangular surface defects are due to threading dislocations. Whereas the step flow progresses in a normal manner at the sites of divergence due to dislocations, at threading dislocations the step progression is prevented in a localized manner, and it is considered that triangular terraces are formed as a result of subsequent steps gaining ground at these loci. Figure 4 (c) shows the morphology after etching of the surface defect areas that have parallel terraces. When the same loci as in Fig. 3 (c) were evaluated, the steps were inflected at the upstream sides of the step flow at the lower ends of the terraces, and at these loci it was shown that two pseudoelliptical etching pits due to basal plane dislocations were superimposed. No other etching pits were found at neighboring areas that included defects. On the basis of these findings, it is considered that crystal defects appearing on the wafer surface are closely linked to surface morphology, and that crystal defects influence step-flow growth.
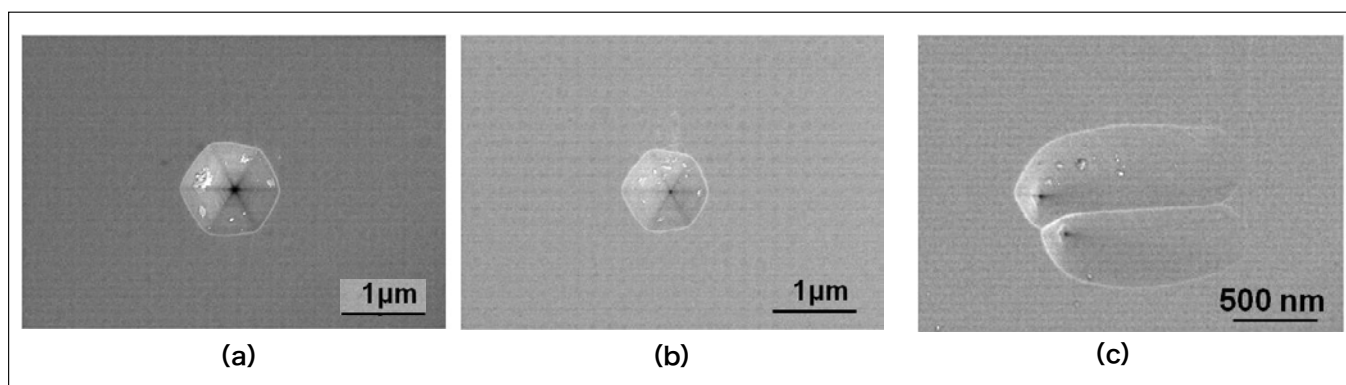
 [12]

Fig. 4 Morphology of surface defects after potassium hydroxide etching
(a) Surface defects with triangular terraces; terrace width: 270 nm
(b) Surface defects with triangular terraces; terrace width: 90 nm
(c) Surface defects with parallel terraces

3. Crystallographic Analysis of Dislocations Using STEM

Inference of dislocation type from etching pit morphology was discussed in the previous section. However, in order to determine the effects on causes of dislocation and on device characteristics, it is necessary to investigate the mode of intracrystalline propagation of dislocations, and the directions of distortion in the crystal lattice at the dislocation loci.

The method in general use for investigating the characteristics of dislocation is cross-sectional transmission electron microscopy (TEM) of the dislocation locus. In evaluation using the TEM in previous use, it was necessary to make observations after processing the samples to a thickness of approximately 100 nm. It is not solely that it was difficult to carry out processing that targeted the dislocation locus, but that there were difficulties with the reliability of evaluation, in that the processing had to be carried out while the direction of intracrystalline propagation of dislocations was unknown, and it was difficult to prepare samples while reliably maintaining the dislocation within the processed sample. While considering the use of samples that are thicker than normal, being 500 nm to 1 μm thick, we tried evaluating crystal defects by means of STEM, which enables evaluation of thicker samples than TEM. The electron-optics systems have different constructions in the cases of STEM and TEM, and even thick samples can be viewed at relatively high contrast using STEM. In the present evaluation, the 200 keV STEM HD-2700 (Hitachi High-Technologies Corporation) was used (Fig. 5). Using this device, in the case of diffraction waves that must be identified for evaluation of dislocation, it is possible to capture images after selective excitation, these being two-beam excitation images, and determination of the crystallographic orientation of dislocations is thus also possible.

Samples were prepared by the microsampling method using the FIB FB2200 (Hitachi High-Technologies Corporation; Fig. 6). This method involves transferring a specified part of the wafer to a raised sample-holder using a fine needle, and then carrying out the processing, while examining the image, and it therefore enables preparation of dislocation-containing samples, with very precise positioning. The sample-holder can be used with both FIB and STEM, and can be moved easily between the appropriate devices. In addition, the tip of a sample-holder has a mechanism with which the orientation of the sample can be changed throughout 360°.

Fig. 5　External appearance of HD-2700

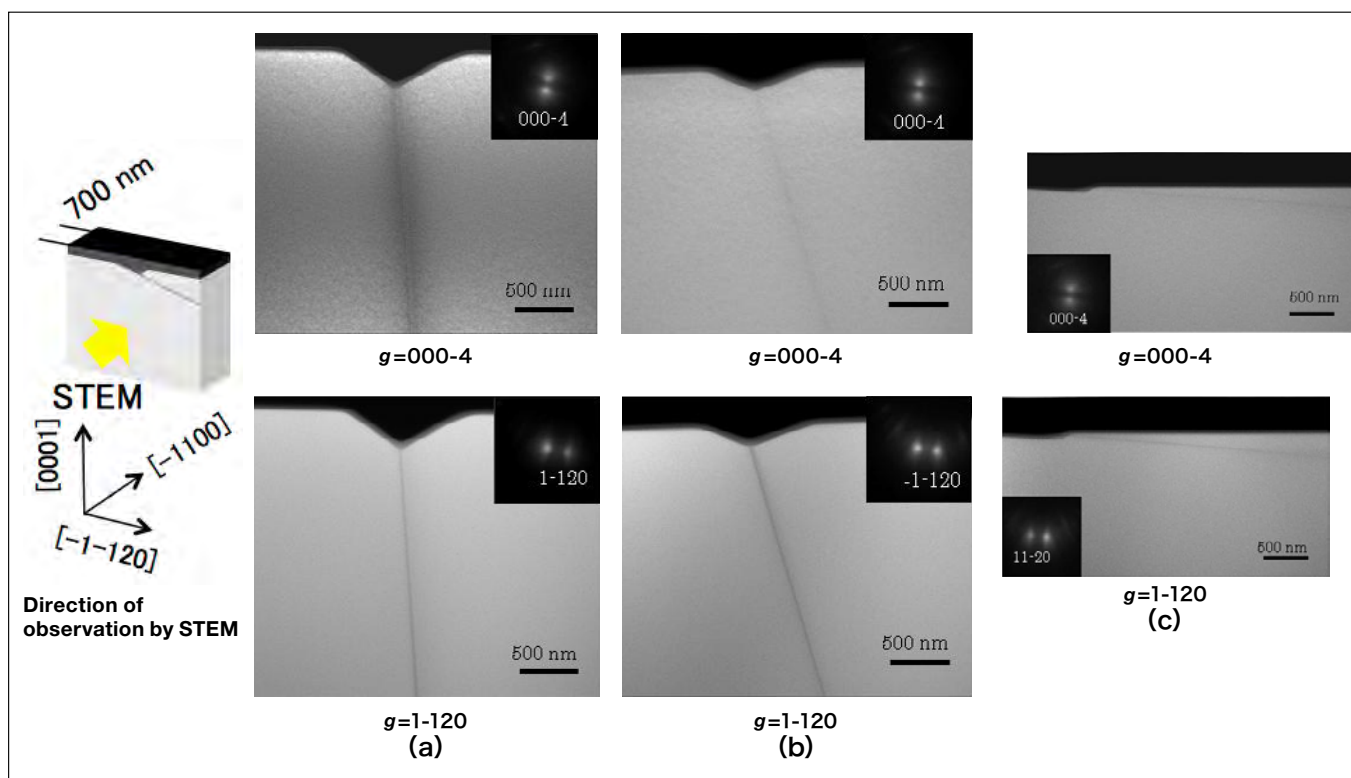**Fig. 6　External appearance of FB2200**

 [14]

Fig. 7   Cross-sectional STEM image of core areas of etching pits
(a) Surface defects with triangular terraces; terrace width: 270 nm
(b) Surface defects with triangular terraces; terrace width: 90 nm
(c) Surface defects with parallel terraces

Figure 7 shows cross-sectional STEM images of the areas of surface defects the evaluation of which is described in the previous section. The direction of observation is [1-100], and the step-flow direction is from right to left, which is the opposite of that in the SEM images. Samples were prepared, each 500 nm thick, targeting the cores of each of the etching pits shown in Fig. 4. It was possible to obtain clear images of all loci, without missing any dislocations. It can be seen that the dislocations in Fig. 7 (a) and (b) are threading dislocations that are propagated in a transverse direction in relation to the wafer surface, and that Fig. 7 (c) shows a basal-plane dislocation that is propagated within the basal plane, at an angle of 4° in relation to the wafer surface. These findings were consistent with the results based on etching pit morphology detailed in the previous section. For each of the images in the figure, the orientation and excitation conditions were changed, and the orientation of the Burger's vector for the relevant dislocation can therefore be determined by comparing these. The Burger's vector is an important parameter expressing the properties of a dislocation, and it shows the orientation of distortion of the crystal surface due to the dislocation. In Fig. 7 (a), dislocations are visible with excitation at both 000-4 and 11-20, and it can be seen that the Burger's vector has the components <0001> and <11-20>. The dislocation in Fig. 7 (b), on the other hand, is invisible and visible with excitation at 000-4 and 11-20, respectively, and it thus has only the <11-20> component, and not the <0001> component. In summary, the dislocation in Fig.7 (a) is a mixed dislocation, combining components of edge and screw dislocations, whereas that in Fig. 7 (b) is an edge dislocation without any screw dislocation components. As far as can be determined from the morphologies of the etching pits in Fig. 4 (a) and (b), it is difficult to identify such differences, and STEM analysis is therefore important for detailed identification of dislocation types. On the other hand, the only Burger's vector of the basal plane dislocation in Fig. 7 (c) was <11-20>. Two superimposed pits can be seen in Fig. 4 (c), but one remaining reason for uncertainty is that only a single dislocation line was found by STEM.

In this context, examination of the sample with transmission from the upper surface was tried. Each of the sample-holders was detached from the STEM device and attached to the FIB device, after which the sample was rotated, the basal part of the sample was shaved, and a rectangular sample with a thickness of 1 μm was prepared from the epitaxial surface. The result of STEM examination of this sample from the epitaxial surface is shown in Fig. 8.

 [15]

Two etching pits are seen to be superimposed, to the left side of the image. Two of the pits extend in the left-to-right direction from the cores to the dark, planar areas, and lamination defects can be seen to be present. Giving consideration to Fig. 7 (c) and 8 together, there is stacking fault aligned with the basal plane, with associated partial dislocations at both ends, and it is considered that, where partial dislocations appear on the wafer surface, two etching pits are superimposed.
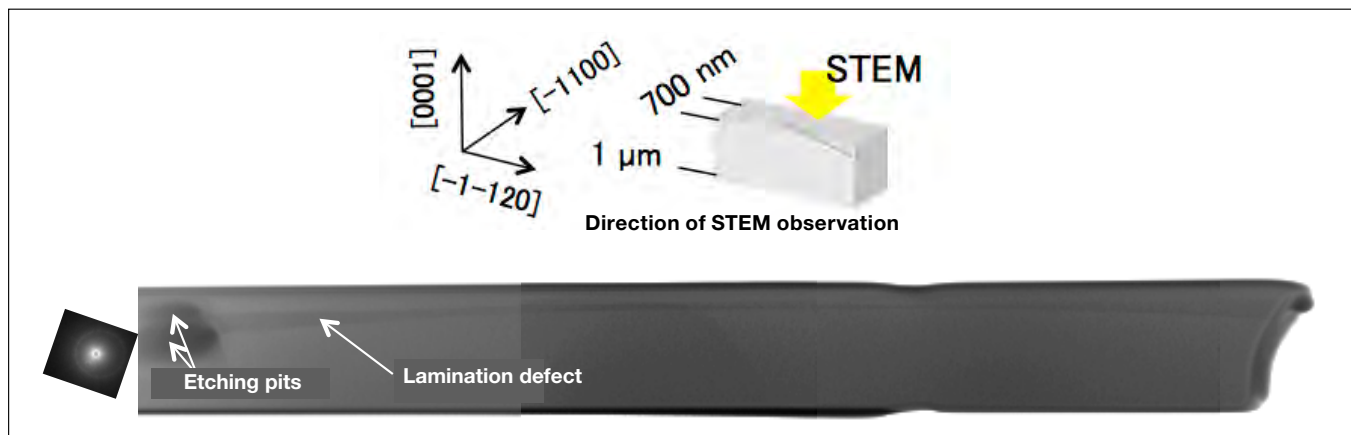

Fig. 8　Planar STEM image of the basal plane dislocation shown in Fig. 7 (c), with zone-axis incidence

4. Closing Remarks

Evaluation of SiC crystal defects using electron microscopy is explained. The effects of dislocations on step-flow growth, and the surface morphology resulting from dislocation types, were elucidated using high-resolution SEM. Together with analyzing the relationships between various wafer dislocations and surface morphology, it is considered necessary to clarify the mechanism by which surface morphology is modified by dislocations. It is hoped that, if these relationships apply generally, high-resolution SEM will make a major contribution to increasing the effectiveness of evaluation of SiC dislocations. Combination of FIB microsampling and STEM observation enables reliable determination of dislocation types, and thus enables evaluation of the three-dimensional structure of crystal defects by multidirectional STEM analysis. It is hoped that electron microscopy techniques such as presented here will contribute to a deeper understanding of SiC crystal defects, and to increasing the performance and reliability of SiC devices.

I would like to thank everyone at Hitachi High-Technologies Corporation for their cooperation with evaluation using electron microscopes in the present research.

References
1) H. Matsusaki et al. ed.: *Semiconductor SiC techniques and applications (ed. 2),* Nikkan Kogyo Shimbun (2011) (Japanese).
2) Y. Orai et al., *Proc. European Conference on Silicon Carbide & Related Materials 2014*, TU-P-35 (2014).
3) T. Sato et al., *Proc. European Conference on Silicon Carbide & Related Materials 2014*, Mo-P-23 (2014).
4) T. Sato et al. *Proc. The 62nd Spring Meeting of Japan Society of Applied Physics*, 11p-P2-7 (2015)(Japanese).
5) K. Kuroda et al., Ext. Abstr. *19th Solid State Device and Materials*, 227 (1987).
6) M. Fukui et al., 14th International Conference on Defects-Recognition, *Imaging and Physics in Semiconductor*, 58 (2011).
7) T. Sato et al., *Materials Science Forum*, 358-361 (2014).